EFFECTS OF ISOLATED BODY AND WING-BODY INTERFERENCE ON ROLLING MOMENT DUE TO SIDESLIP: L_v (WITH ADDENDUM A FOR NACELLE EFFECTS)

1. NOTATION AND UNITS

The derivative notation used is that proposed in ARC R&M 3562 (Hopkin, 1970) and described in Item No. 86021. Coefficients and aeronormalised derivatives are evaluated in aerodynamic body axes with origin at the aircraft centre of gravity, assumed to lie on the locus of centroids of the body cross sections and in the plane normal to that locus that passes through the quarter-chord point of the wing aerodynamic mean chord, and with the wing span as the characteristic length. The derivative L_v is often written as $\partial C_l/\partial\beta$ or $C_{l\beta}$ in other systems of notation, but attention must be paid to the reference dimensions used and it is to be noted that a constant datum value of V is employed in the Hopkin system.

		SI	*British*
A	aspect ratio, b^2/S		
b	wing span	m	ft
C_L	lift coefficient of wing-body combination		
C_l	rolling moment coefficient, $\mathscr{L}/\frac{1}{2}\rho V^2 Sb$		
d	maximum diameter for body of circular cross-section	m	ft
$f(A)$	aspect ratio correction factor		
H	height of ellipse equivalent to body reference cross-section (see Section 2)	m	ft
h_0	vertical distance of quarter-chord point of wing centre-line chord from centroid of body reference cross-section, positive if below centroid and negative if above (see Section 2)	m	ft
h	wing vertical position relative to body, defined by Equation (4.1)	m	ft
$\mathscr{L}$	rolling moment	N m	lbf ft
L_v	aero-normalised rolling moment derivative due to sideslip, $(\partial\mathscr{L}/\partial v)/\frac{1}{2}\rho VSb$		
$(L_v)_b$	isolated body contribution to L_v		
$(L_v)_h$	that part of L_v due to interference arising from vertical position of wing on body, $(L_v)_{w+b}-(L_v)_w-(L_v)_b$		
$(L_v)_w$	isolated gross wing contribution to L_v (see Item Nos Aero A.06.01.03, Aero A.06.01.09 and 80033)		
$(L_v)_{w+b}$	wing-body combination contribution to L_v		

Issued June 1973
Reprinted with Amendments A to C, March 1999 – 20 pages
This page Amendment C

l_b	body length	m	ft
S	gross wing area	m^2	ft^2
S_b	maximum cross-sectional area of body	m^2	ft^2
V	velocity of aircraft relative to air	m/s	ft/s
v	sideslip velocity	m/s	ft/s
W	width of body reference cross-section (see Section 2)	m	ft
α_b	body incidence measured from body zero-lift value	degree	degree
β	sideslip angle, $\sin^{-1}(v/V) \approx v/V$	rad	rad
Γ	dihedral angle, defined as angle between wing reference plane and projection of quarter-chord line on plane perpendicular to wing centre-line chord; the wing reference plane is that plane normal to plane of symmetry and containing wing centre-line chord	degree	degree
κ	factor in Equation (4.1)	$degree^{-1}$	$degree^{-1}$
$\Lambda_{¼}$	angle of sweepback of quarter-chord line	degree	degree
λ	taper ratio (ratio of wing tip chord to wing centre-line chord)		
ρ	density of air	kg/m^3	$slug/ft^3$

2. WING-BODY GEOMETRY

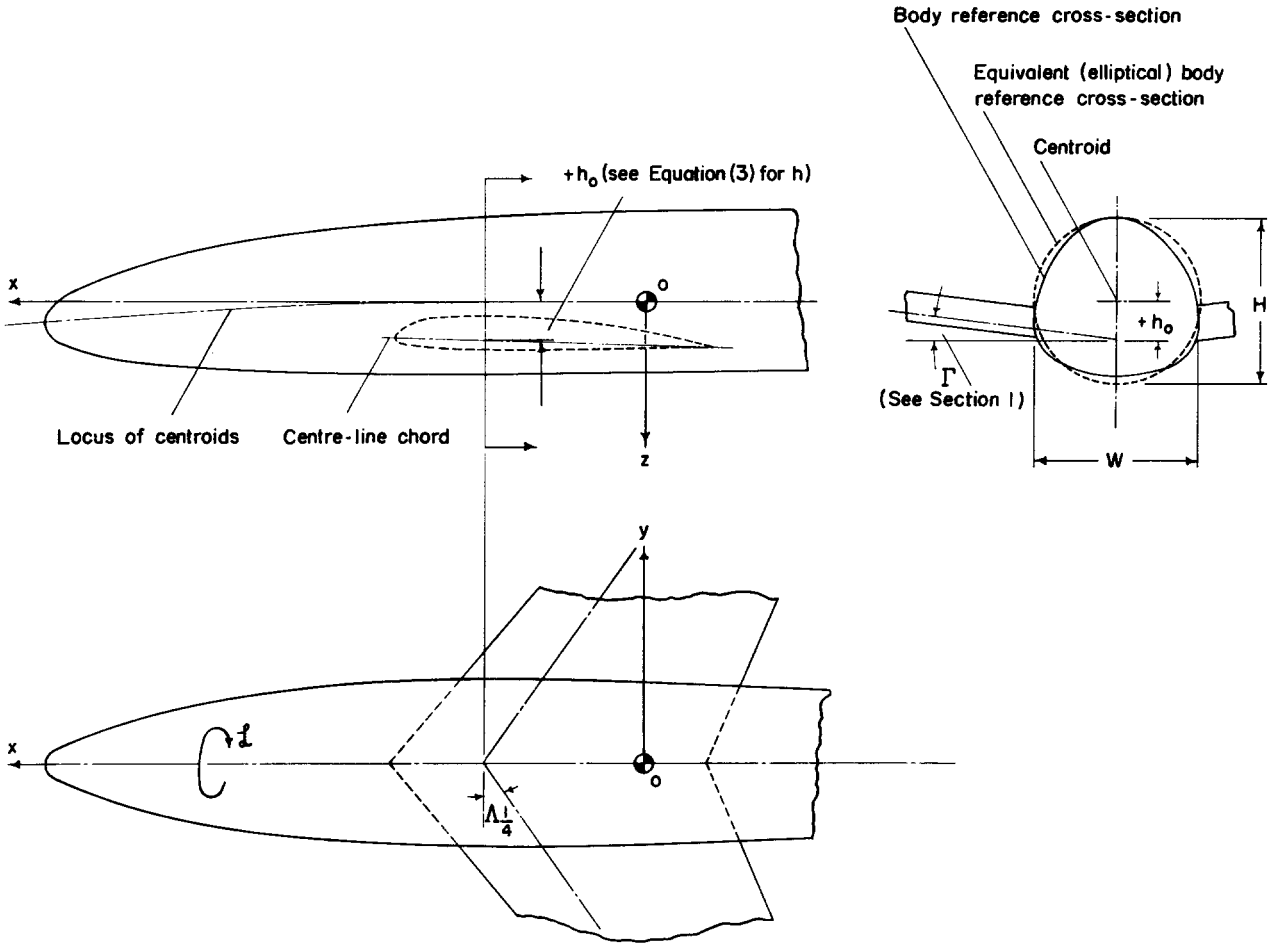

2.1 Body Reference Cross-section

The body reference cross-section is that section in the Oyz plane containing the quarter-chord point of the wing centre-line chord.

2.2 Equivalent (Elliptical) Body Reference Cross-section

The equivalent (elliptical) body reference cross-section is that ellipse having the same area, width and centre of area as the body reference cross-section. The height of the ellipse is

$$H = \frac{4}{\pi W} \times \text{area of body reference cross-section}\,.$$

3. INTRODUCTION

The data given in this Item provide a means of estimating the effect on the rolling moment derivative due to sideslip, L_v, of adding a body to a gross wing. The data apply to low speeds and to lift coefficients for which the flow over the wing-body combination remains fully attached (see Item No. 66033 for wings with symmetrical sections). The gross wing contribution, $(L_v)_w$, may be obtained from Item Nos Aero A.06.01.03, Aero A.06.01.09 and 80033. The fin and rudder contribution to L_v may be obtained from Item No. 70006. Information on the effect on L_v of mounting jet-engine nacelles on the aft portion of the body or below the wing is given in Addendum A of this Item.

Wind-tunnel tests show that when a wing and body are in combination the total value of L_v, *i.e.* $(L_v)_{w+b}$, is not equal to the sum of the contributions arising from the gross wing and body when tested in isolation, thus demonstrating the presence of interference effects between the wing and body. In the linear lift range these interference effects are primarily due to the vertical position of the wing with respect to the body although there is some evidence to suggest that there can be secondary effects which are lift-dependent, arising from the longitudinal position of the wing relative to the body (see Section 4.2).

The interference arising from the vertical position of the wing with respect to the body, $(L_v)_h$, is caused by changes in the local wing incidence induced by the cross-flow around the body. Theoretical treatments of this effect are given in Derivations 5 and 9, and methods from these two Derivations are used herein (see Section 4.1).

The isolated body contribution, $(L_v)_b$, is usually small compared with the isolated wing and fin and rudder contributions. A simple method of estimating $(L_v)_b$ is given in Section 5.

The total effect, on the rolling moment due to sideslip, of adding a body to a wing is therefore estimated from this Item as

$$(L_v)_h + (L_v)_b . \tag{3.1}$$

The wing-body combination contribution to L_v may be obtained by adding the gross wing contribution to the above expression, *i.e.*

$$(L_v)_{w+b} = (L_v)_w + (L_v)_h + (L_v)_b . \tag{3.2}$$

4. INTERFERENCE COMPONENTS

4.1 Due to Vertical Position of Wing on Body, $(L_v)_h$

Figure 1a presents, for $A = 6$, the parameter $|(L_v)_h|/(1 + W/H)f(A)$ plotted against $|h/H|$ for various values of H/b. It should be noted that $(L_v)_h$ values obtained from this Figure adopt the same sign as h/H. Figure 1b gives the aspect ratio correction factor, $f(A)$, as a function of aspect ratio.

Figure 1a was obtained by the method of Derivation 5, which, by making certain approximations, allows a simpler solution than that of Derivation 9. Also the method of Derivation 5 happens to provide better agreement with available experimental data than that of Derivation 9, especially for the larger values of H/b. Figure 1b was obtained from Derivation 9.

The curves in Figures 1a and 1b were derived, for incompressible fully-attached flow, on the assumption that a body of infinite length and constant elliptical cross-section is in combination with an unswept wing

of elliptic planform with no dihedral or twist. The data can be applied, however, to wing-body combinations with finite body lengths* , other body cross-sections and other wing planforms, both with and without dihedral as shown later.

If the shape of the body reference cross-section (see Section 2.1) departs from the elliptical section assumed in the Derivation of Figures 1a and 1b, empirical evidence (Derivation 9) suggests that the actual cross-section in the reference plane should be replaced by an equivalent, elliptical, section (see Section 2.2).

In order to determine the wing vertical position, h, relative to the equivalent body reference cross-section, in terms of the height of that section, H, for the general case of a wing with dihedral, the following expression should be used;

$$\frac{h}{H} = \frac{h_0}{H} - \kappa\Gamma, \tag{4.1}$$

where Γ is the dihedral angle (assumed constant across the wing semi-span) in degrees. The parameter κ (from Derivation 9) is given in Figure 2 for ranges of values of $|h_0/H|$ and H/b. It will be seen that when the dihedral angle is zero the wing vertical position reduces to h_0, the vertical distance of the quarter-chord point of the wing centre-line chord from the centroid of the body reference cross-section.

4.1.1 Comparison with experimental data

Agreement with experimental data for $(L_v)_h$ for wing-body combinations in which the wing has zero dihedral (Derivations 1 to 4, 10, 11, 14 and 17) is generally within about ±0.015. The test data cover the ranges $2.3 \le A \le 6.4$, $0 \le \lambda \le 1$, $0 \le \Lambda_{¼} \le 52°$, $-0.42 \le h_0/H \le 0.44$ †, $0.11 \le H/b \le 0.24$, $0.54 \le W/H \le 1$ and $-0.4 \le C_L \le 0.8$. This agreement with the experimental data is a little worse than the experimental scatter in only a few cases. The experimental data indicate no consistent trends due to wing taper or sweep, and such effects are small and submerged in the general scatter.

Agreement with experimental data for $(L_v)_h$ for wing-body combinations in which the wing has dihedral (Derivations 1, 2, 4, 6 and 8) is again generally within ±0.015. The test data cover the ranges $5.2 \le A \le 6.9$, $0.25 \le \lambda \le 1.0$, $1.5° \le \Gamma \le 6°$, $0 \le \Lambda_{¼} \le 5°$, $-0.59 \le h/H \le 0.39$, $0.11 \le H/b \le 0.19$, $0.54 \le W/H \le 1.0$ and $-0.4 \le C_L \le 0.8$.

The experimental data from the above-mentioned Derivations related (with one exception) to bodies of either elliptical or circular cross-section. The data from Derivation 1 relate to two bodies with cross-sections grossly different from elliptical, but good agreement is obtained with values from this Item when equivalent, elliptical, sections (see Section 2.2) are used.

4.1.2 The effect of flap deflection

The limited experimental data (Derivations 3, 6, 8, 10 and 11) for the effect of flap deflection are generally small in magnitude, but their trends are inconsistent.

* Provided that at least a quarter of the body length lies ahead of the quarter-chord point of the wing centre-line chord (see Derivation 9).

† Although the curves in Figure 1a have only been taken up to $|h/H| = 0.6$ the calculations have been extended up to 1.0 in Derivation 9. Experimental data from Derivation 7 for parasol-wing configurations ($|h_0/H|$ up to 0.8) are shown in Derivation 9 to substantiate the theoretical calculations for these configurations.

4.2 Due to Longitudinal Position of Wing on Body

There is evidence (Derivations 3, 10 to 14, 16 and 17) to suggest that, even for circular-section bodies with wings mounted in the mid-height position with flaps undeflected, there exist interference effects which are lift-dependent. These effects have been ascribed (Derivation 18) to the reduction of the wing local sideslip angle due to lateral distortion of the flow field over the wing by the presence of the body. Various attempts were made to correlate these effects, but the best of these was only moderately successful in that it left very considerable scatter in the data. This was largely due to the fact that the interference effects to be correlated were small, and indeed their magnitudes were less than the scatter of the $(L_v)_h$ data correlation over the linear-lift range.

With regard to mid-mounted wings with large deflections of trailing-edge flaps (characteristic of the landing configuration) Derivations 10 and 16 indicate that the lift-dependent interference effects are negligible.

5. ISOLATED BODY CONTRIBUTION, $(L_v)_b$

The isolated body contribution to L_v is generally small compared with the wing and fin and rudder contributions. Analysis of experimental data for $(L_v)_b$ (Derivations 8 and 13 to 17) shows that it may be estimated, for bodies of circular cross-section with ratios of length/maximum diameter in the range $5 \le l_b/d \le 12$ and body incidences in the range $-8 \le \alpha_b \le 12°$, from the expression

$$\frac{(L_v)_b}{\alpha_b} = -0.014 \frac{l_b}{b} \frac{S_b}{S} \text{ degree}^{-1}, \tag{5.1}$$

in which the body incidence, α_b, is measured from its zero-lift value.

Equation (5.1) was found to represent the experimental data used in its derivation to within ± 0.0003. Caution should be exercised in applying Equation (5.1) to bodies outside the ranges of l_b/d and α_b from which it was derived. For bodies of other than circular cross-section it is tentatively suggested that the equivalent height be used in place of the maximum diameter. In applying Equation (5.1) to bodies of other than circular cross-section and for which the maximum cross-sectional area is not easily obtainable, it is acceptable to take S_b as the area of the body reference cross-section.

6. DERIVATION

The Derivation lists selected sources that have assisted in the preparation of this Item.

1. IRVING, H.B. BATSON, A.S. WARSAP, J.H. — Model experiments on the rolling moment due to sideslip of tapered wing monoplanes. ARC R & M 2019, 1939.
2. BAMBER, M.J. HOUSE, R.O. — Wind-tunnel investigation of effect of yaw on lateral-stability characteristics. II – rectangular NACA 23012 wing with a circular fuselage and a fin. NACA tech. Note 730, 1939.
3. HOUSE, R.O. WALLACE, A.R. — Wind-tunnel investigation of effect of interference on lateral-stability characteristics of four NACA 23012 wings, an elliptical and a circular fuselage and vertical fins. NACA Rep. 705, 1940.
4. JACOBS, W. — Berechnung des Schieberollmomentes für Flügel/Rumpfanordnungen. Jahrbuch 1941 der d.Lff., S.I.165.

5.	MULTHOPP, H.	Zur Aerodynamik des Flugzeugrumpfes. Luftfahrtforschung, Vol. 18, No. 2/3, 1941. (Translated in RTP Trans. 1220, ARC 5263, 1941).
6.	RECANT, I.G. WALLACE, A.R.	Wind-tunnel investigation of effect of yaw on lateral-stability characteristics. III – symmetrically tapered wing at various positions on circular fuselage with and without a vertical tail. NACA tech. Note 825, 1941.
7.	MÖLLER, W.	Systematische Sechskomponentenmessungen am Flügel/ Rumpfanordnungen. Jahrbuch 1942 der d.Lff., S.I.336.
8.	WALLACE, A.R. TURNER, T.R.	Wind-tunnel investigation of effect of yaw on lateral-stability characteristics. V – symmetrically tapered wing with a circular fuselage having a horizontal and a vertical tail. NACA ARR 3F23 (TIB 456), 1943.
9.	LEVACIC, I.	Rolling moment due to sideslip. Part III.A. The effect of wing body arrangement. B. The effect of tail unit. RAE Rep. Aero. 2139, 1946.
10.	SALMI, R.J. CONNER, D.W. GRAHAM, R.R.	Effects of a fuselage on the aerodynamic characteristics of a 42° sweptback wing at Reynolds numbers to 8,000,000. NACA RM L7E13 (TIB 1185), 1947.
11.	SALMI, R.J.	Yaw characteristics of a 52° sweptback wing of NACA 64-112 section with a fuselage and with leading-edge and split flaps at Reynolds numbers from 1.93×10^6 to 6.00×10^6. NACA RM L8H12 (TIB 1984), 1948.
12.	LETKO, W. WOLHART, W.D.	Effect of sweepback on the low-speed static and rolling stability derivatives of thin tapered wings of aspect ratio 4. NACA RM L9F14 (TIB 2288), 1949.
13.	QUEIJO, M.J. WOLHART, W.D.	Experimental investigation of the effect of vertical-tail size and length and of fuselage shape and length on the static lateral stability characteristics of a model with 45° sweptback wing and tail surfaces. NACA Rep.1049. 1950.
14.	GOODMAN, A.	Effects of wing position and horizontal-tail position on the static stability characteristics of models with unswept and 45° sweptback surfaces with some reference to mutual interference. NACA tech. Note 2504, 1951.
15.	KUHN, R.E. FOURNIER, P.G.	Wind-tunnel investigation of the static lateral stability characteristics of wing-fuselage combinations at high subsonic speeds. Sweep series. NACA RM L52G11a (TIB 3330), 1952.
16.	GRINER, R.F.	Static lateral stability characteristics of an airplane model having a 47.7° sweptback wing of aspect ratio 6 and the contribution of various model components at a Reynolds number of 4.45×10^6. NACA RM L53G09 (TIB 3885), 1953.
17.	GOODMAN, A. THOMAS, D.F.	Effects of wing position and fuselage size on the low-speed static and rolling stability characteristics of a delta-wing model. NACA Rep. 1224, 1953.
18.	POLHAMUS, E.C. SLEEMAN, W.C.	The rolling moment due to sideslip of swept wings at subsonic and transonic speeds. NASA tech. Note D–209, 1954.

7. EXAMPLE

Estimate the effect of the body (neglecting tail interference effects) on the rolling moment derivative due to sideslip for a large high wing transport aircraft in the landing approach, for which $\alpha_b = 3$ degrees. The body reference cross-section (of area 42.4 m^2) is shown as a half-view in the sketch which includes some of the relevant dimensions. The other necessary geometrical parameters for the wing and body are

$$A = 8\,,\ b = 75 \text{ m},\ S = 703 \text{ m}^2\,,\ l_b = 77 \text{ m}.$$

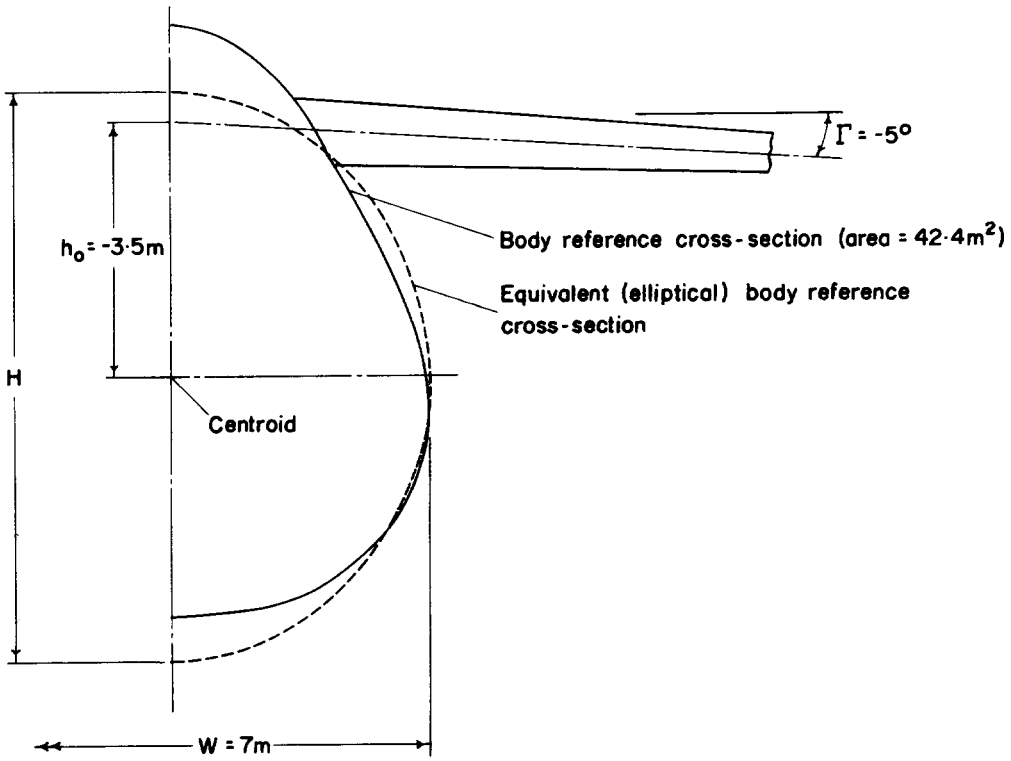

From Section 2.2, the value of H is calculated from

$$H = \frac{4}{\pi W} \times \text{area of body reference cross-section}$$

$$= \frac{4}{\pi W} \times 42.4 = 7.7 \text{ m}.$$

From Figure 2, with $|h_0/H| = |-3.5/7.7| = 0.455$ and $H/b = 7.7/75 = 0.103$, $\kappa = 0.0093$ degree^{-1}.

Thus from Equation (4.1),

$$\frac{h}{H} = -0.455 - 0.0093 \times (-5)$$

$$= -0.408\,.$$

From Figure 1a, with $h/H = -0.408$ and $H/b = 0.103$,

$$\frac{(L_v)_h}{\left(1+\frac{W}{H}\right) f(A)} = -0.0136.$$

From Figure 1b, with $A = 8$,

$$f(A) = 1.10.$$

Hence, for $W/H = 7/7.7 = 0.909$,

$$(L_v)_h = \frac{(L_v)_h}{\left(1+\frac{W}{H}\right) f(A)} \times \left(1+\frac{W}{H}\right) f(A)$$
$$= -0.0136 \times (1 + 0.909) \times 1.10$$
$$= -0.0286.$$

If Equation (5.1) is assumed to apply to bodies with a typical cross-section as shown in the sketch, then, for $\alpha_b = 3°$,

$$(L_v)_b = -0.014 \frac{l_b}{b} \frac{S_b}{S} \times \alpha_b = -0.014 \times \frac{77}{75} \times \frac{42.4}{703} \times 3$$
$$= -0.0026,$$

where S_b is taken as the area of the body reference cross-section.

Therefore, the total body effect on L_v is given by Equation (3.1) as

$$(L_v)_h + (L_v)_b = -0.0286 - 0.0026$$
$$= -0.031.$$

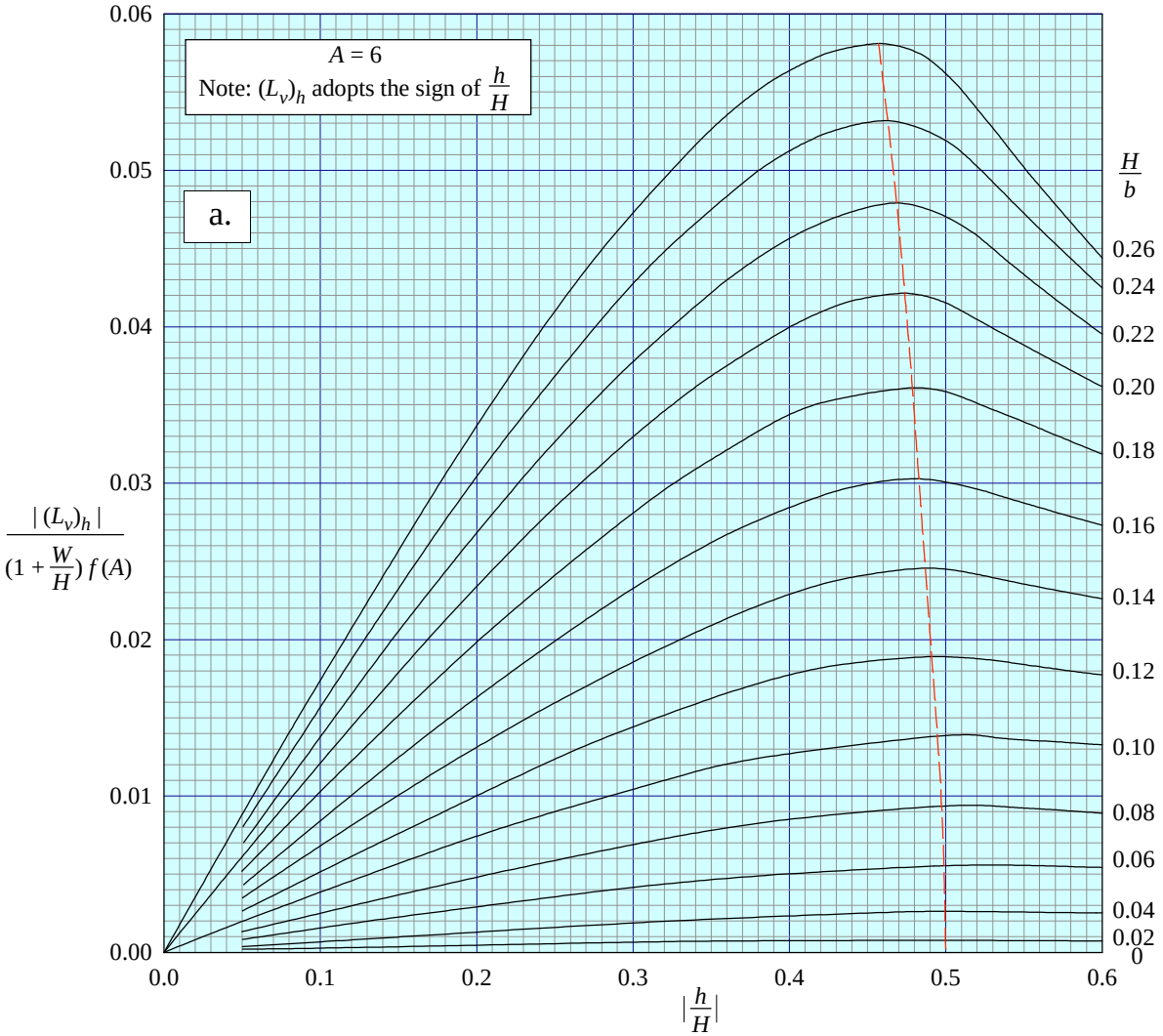
A = 6
Note: $(L_v)_h$ adopts the sign of $\frac{h}{H}$
a.
$\frac{|(L_v)_h|}{(1+\frac{W}{H})f(A)}$
$|\frac{h}{H}|$
$\frac{H}{b}$
0.26
0.24
0.22
0.20
0.18
0.16
0.14
0.12
0.10
0.08
0.06
0.04
0.02
0
0.00
0.01
0.02
0.03
0.04
0.05
0.06
0.0
0.1
0.2
0.3
0.4
0.5
0.6

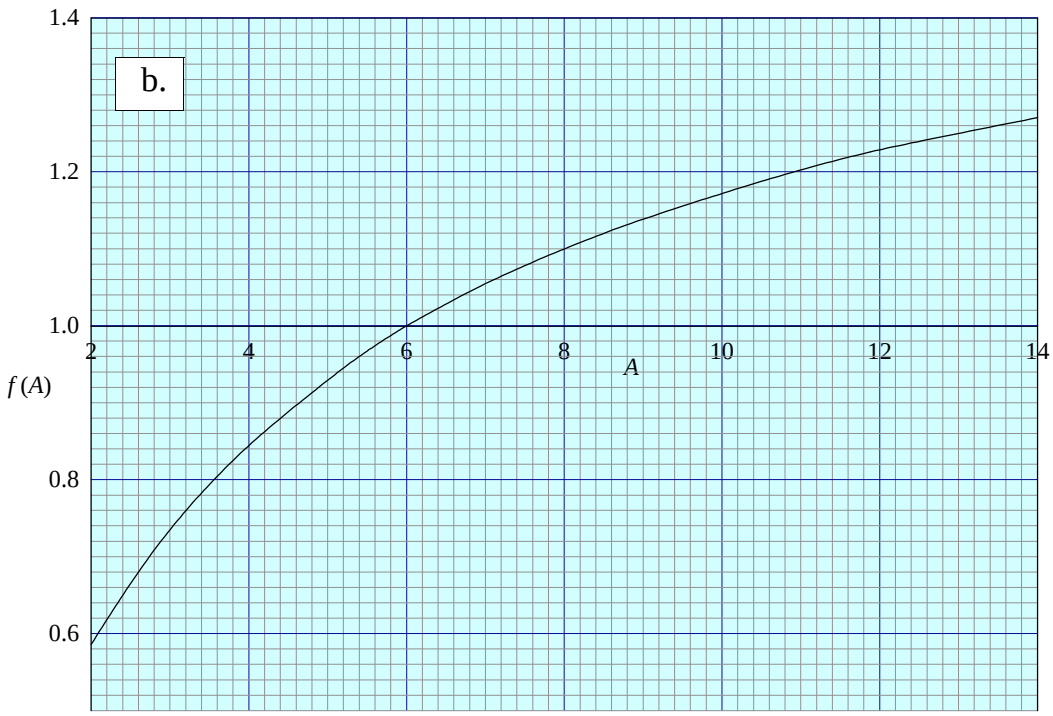
b.
$f(A)$
A
0.6
0.8
1.0
1.2
1.4
2
4
6
8
10
12
14

FIGURE 1

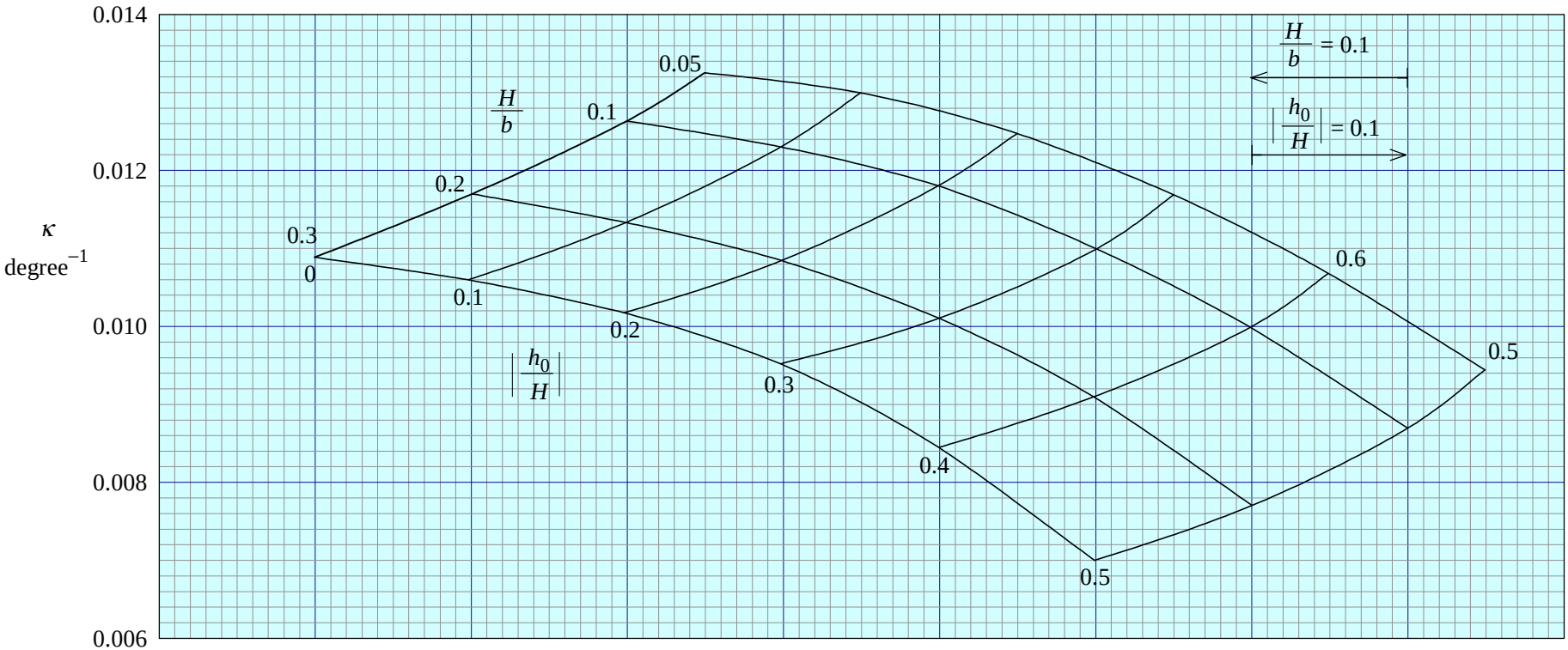
0.014
0.012
0.010
0.008
0.006
κ
degree^{-1}
$\frac{H}{b}$
0.05
0.1
0.2
0.3
0
0.1
0.2
0.3
0.4
0.5
0.6
0.5
$\left|\frac{h_0}{H}\right|$
$\frac{H}{b}$ = 0.1
$\left|\frac{h_0}{H}\right|$ = 0.1

FIGURE 2

THIS PAGE INTENTIONALLY BLANK

ADDENDUM A EFFECT OF JET-ENGINE NACELLES

A1. ADDITIONAL NOTATION AND UNITS (see Sketch A1.1)

		SI	*British*
$(L_v)_n$	contribution to L_v from pair of nacelles, one on each half wing		
$[(L_v)_n]_{zT}$	theoretical contribution to $(L_v)_n$ due to antisymmetric incidence induced across wing span by nacelles		
l_n	overall length of nacelle	m	ft
s	wing semi-span	m	ft
s_n	spanwise distance from body centre-line to nacelle centre-line	m	ft
$w_{n\,max}$	maximum width of nacelle	m	ft
$w_{n\,e}$	nacelle exit diameter	m	ft
z_n	distance of nacelle centre-line below wing-pylon junction	m	ft
z_1	distance of nacelle centre-line below moment reference point	m	ft

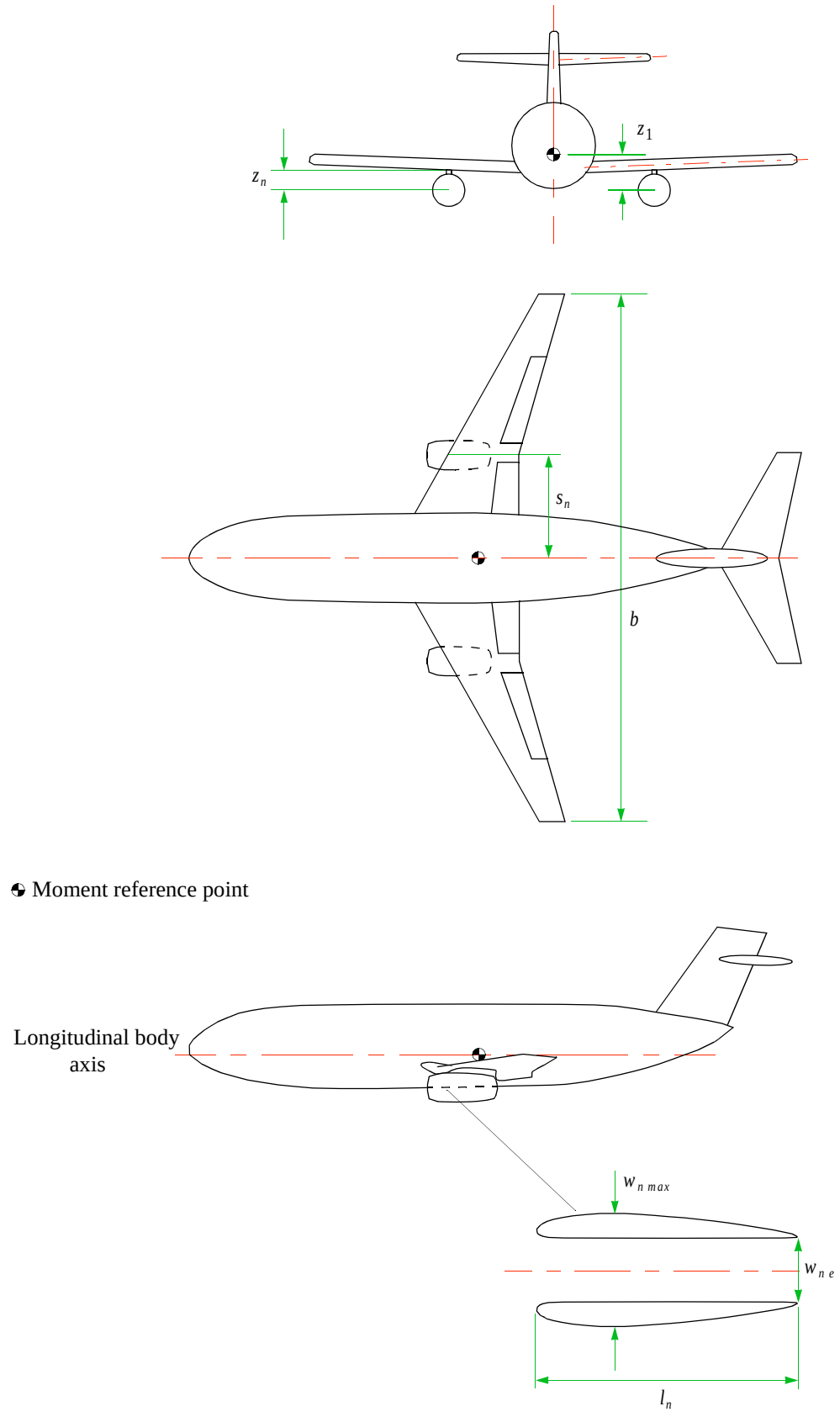
z_1
z_n
s_n
b
Moment reference point
Longitudinal body axis
$w_{n\,max}$
$w_{n\,e}$
l_n

Sketch A1.1

A2. INTRODUCTION

A limited number of wind-tunnel data are available for aircraft models, typical of civil jet-transports, which have been tested both with and without free-flow nacelles of the type customarily fitted in wind-tunnel tests to simulate the presence of jet-engine nacelles. This enables some guidance to be given on the effect of jet-engine nacelles on L_v, but it is emphasised that the range of the experimental data is limited and any estimates of nacelle effects must be used with caution.

A3. REAR-BODY MOUNTED NACELLES

An examination of wind-tunnel data for three low-wing aircraft with wing aspect ratios in the range 7 to 7.5 indicates that nacelles mounted on the rear part of the body have very little effect on L_v. This appears to be true whether or not the model has a tailplane and fin, but significant interference effects between the nacelles and tail surfaces cannot be ruled out.

A4. UNDER-WING MOUNTED NACELLES

Wind-tunnel data for nacelles mounted on under-wing pylons are available from Derivations A1 to A3 for a small number of tests on both high-wing and low-wing multi-engine aircraft with wing aspect ratios in the range 7.5 to 10.

The nacelle-induced rolling-moment sideslip derivative arises from two causes. One contribution comes directly from the sideforce on the nacelle/pylon due to the flow field of the wing and the other from the antisymmetric incidence induced across the wing span by the nacelles.

For a pair of nacelles, one mounted on each half-wing, the best correlation of the available data has been found to be

$$(L_v)_n = -\frac{z_1}{b}(Y_v)_n + 0.86[(L_v)_n]_{zT} \qquad \text{(A4.1)}$$

where $(Y_v)_n$ is the nacelle/pylon sideforce derivative from Addendum A of Item No. 79006 (Derivation A4),

$$(Y_v)_n = -\pi w_{n\,max}^2 \left(\frac{z_n + 0.5 w_{n\,max}}{w_{n\,max}}\right)^{1.5} \Big/ S, \qquad \text{(A4.2)}$$

which is associated with the rolling moment arm z_1, the distance of the nacelle centre-line below the moment reference point, and $[(L_v)_n]_{zT}$, is the theoretical contribution from the induced antisymmetric incidence loading as predicted in Derivation 9, which is factored by an empirical constant of 0.86.

Figure A1 presents $-[(L_v)_n]_{zT}/f(A)(w_{n\,max}/s)^2$ as a function of s_n/s and z_n/s where s_n is the distance of the nacelle centre line away from the plane of symmetry and z_n is the distance of the nacelle centre line below the wing. The wing aspect-ratio correction factor, $f(A)$, is the same as that used for a wing-fuselage combination, which is given in Figure 1b.

Sketch A4.1 compares predicted and experimental values of $\Sigma(L_v)_n$, (for a moment reference point close to the body longitudinal axis), where Σ denotes a summation of two pairs for four-nacelle configurations.

Table A4.1 shows ranges of geometric parameters covered by the experimental data.

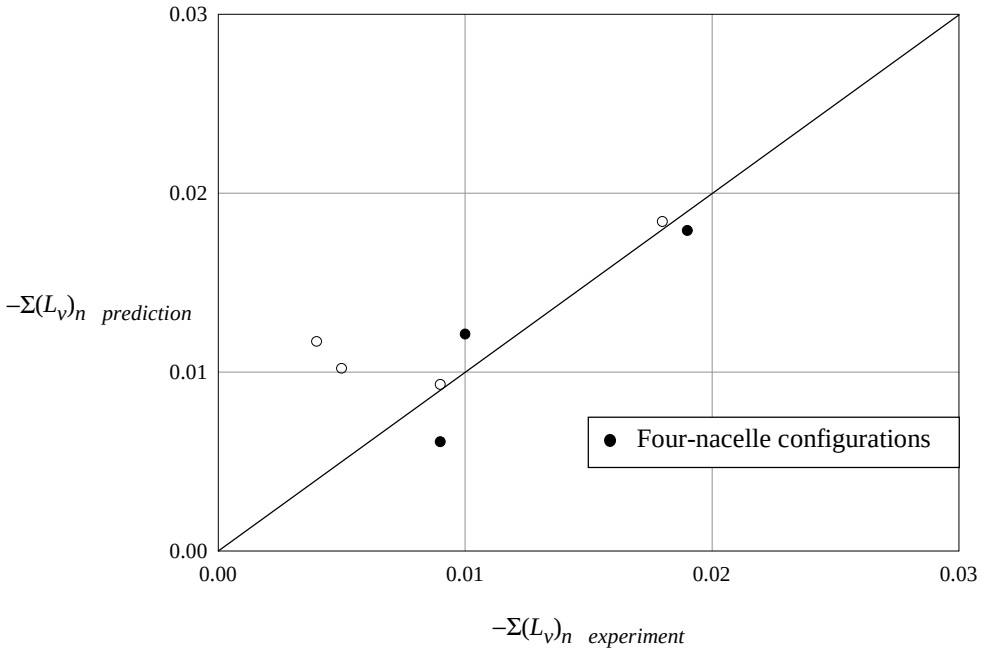

Sketch A4.1

TABLE A4.1

Parameter	*Range*
A	7.5 to 10
l_n/s	0.16 to 0.30
$l_n/w_{n\,max}$	1.6 to 2.7
s_n/s	0.29 to 0.52
$w_{n\,e}/s$	0.055 to 0.092
$w_{n\,max}/s$	0.092 to 0.13
$w_{n\,e}/w_{n\,max}$	0.58 to 0.73
z_n/s	0.056 to 0.13
$(z_n - 0.5w_{n\,max})/w_{n\,max}$	0.2 to 0.8
$(z_n + 0.5w_{n\,max})/w_{n\,max}$	1.2 to 1.8
z_1/s	–0.014 to 0.072

A5. DERIVATION

The Derivation lists selected sources that have assisted in the preparation of this Addendum.

A1.	BAe	Unpublished wind-tunnel data from British Aerospace, Aircraft Group, Hatfield-Chester and Weybridge-Bristol Divisions.
A2.	ARA	Unpublished wind-tunnel data from Aircraft Research Association.
A3.	MORGAN, H.L. PAULSON, J.W.	Low-speed aerodynamic performance of a high-aspect-ratio supercritical-wing transport model equipped with full-span slat and part-span double-slotted flaps. NASA tech. Paper 1580, 1979.
A4.	ESDU	Wing-body yawing moment and sideforce derivatives due to sideslip: N_v and Y_v (With Addendum A for nacelle effects). ESDU International, Item No. 79006, 1979.

A6. EXAMPLE

Calculate the nacelle contribution to the derivative L_v for the configuration shown in Sketch A6.1. The wing reference area is 194.3 m^2 and the aspect ratio is 7.59.

From Equation (A4.2)

$$
\begin{aligned}
(Y_v)_n &= -\pi w_{n\,max}^2 \left(\frac{z_n + 0.5 w_{n\,max}}{w_{n\,max}} \right)^{1.5} \Big/ S \\
&= -\pi 2.25^2 \left(\frac{1.38 + 0.5 \times 2.25}{2.25} \right)^{1.5} \Big/ 194.3 \\
&= -0.0962 \, .
\end{aligned}
$$

From Figure A1, for $s_n/s = 7.6/(38.4/2) = 0.396$ and $z_n/s = 1.36/(38.4/2) = 0.0708$,

$$
\frac{-[(L_v)_n]_{zT}}{f(A)(w_{n\,max}/s)^2} = 1.073
$$

so that with $f(A) = 1.08$ for $A = 7.59$ from Figure 1b,

$$
\begin{aligned}
[(L_v)_n]_{zT} &= -1.073 f(A)(w_{n\,max}/s)^2 \\
&= -1.073 \times 1.08 \times (2.25/(38.4/2))^2 \\
&= -0.0159 \, .
\end{aligned}
$$

Therefore, from Equation (A4.1)

$$
\begin{aligned}
(L_v)_n &= -\frac{z_1}{b} (Y_v)_n + 0.86[(L_v)_n]_{zT} \\
&= -\left(\frac{2.48}{38.4} \right)(-0.0962) + 0.86(-0.0159) \\
&= 0.00621 - 0.01367 \\
&= -0.00746 \, .
\end{aligned}
$$

Thus the contribution of the nacelles to the lateral stability derivative L_v is

$$
(L_v)_n = -0.0075 \, .
$$

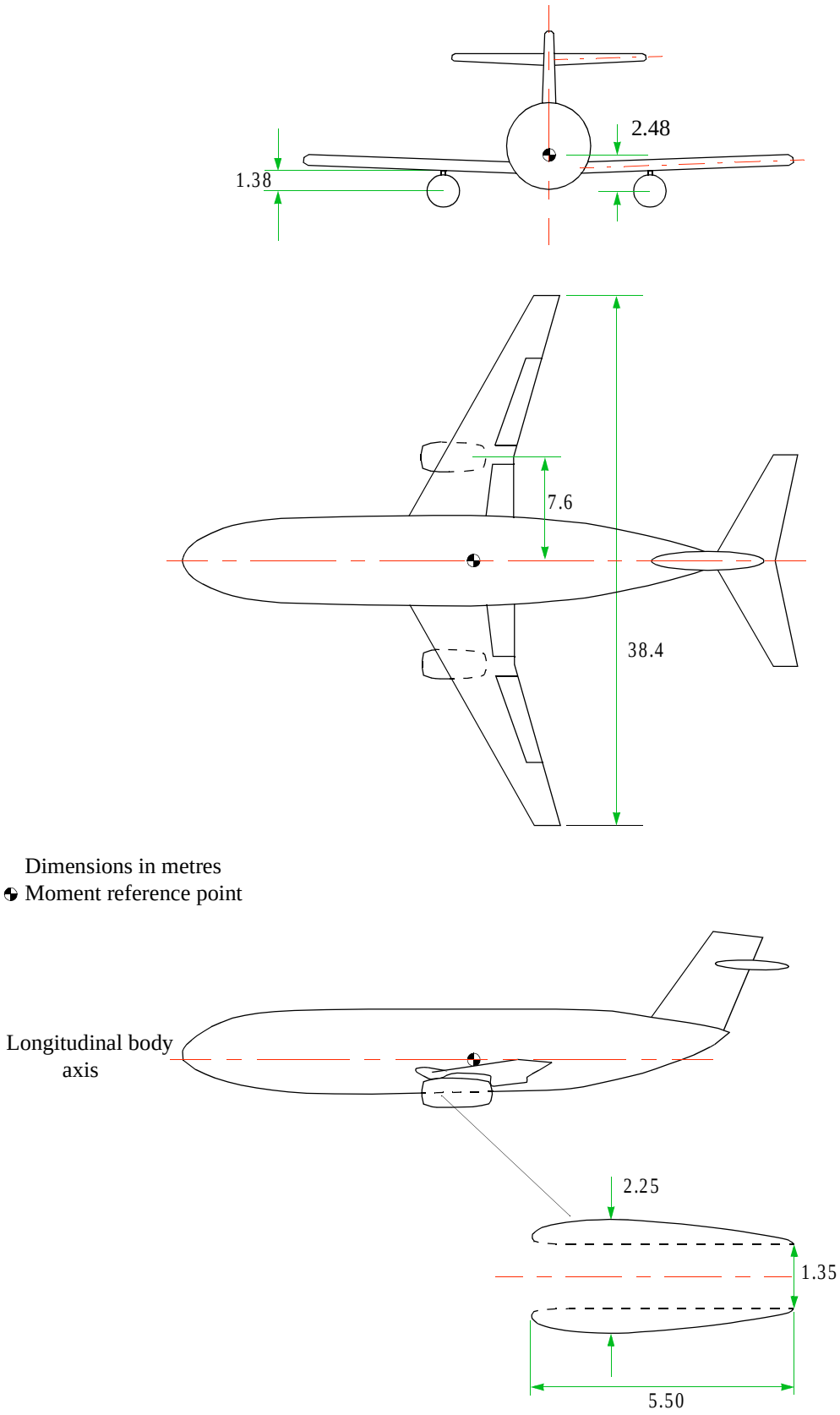

Sketch A6.1 Aircraft Geometry

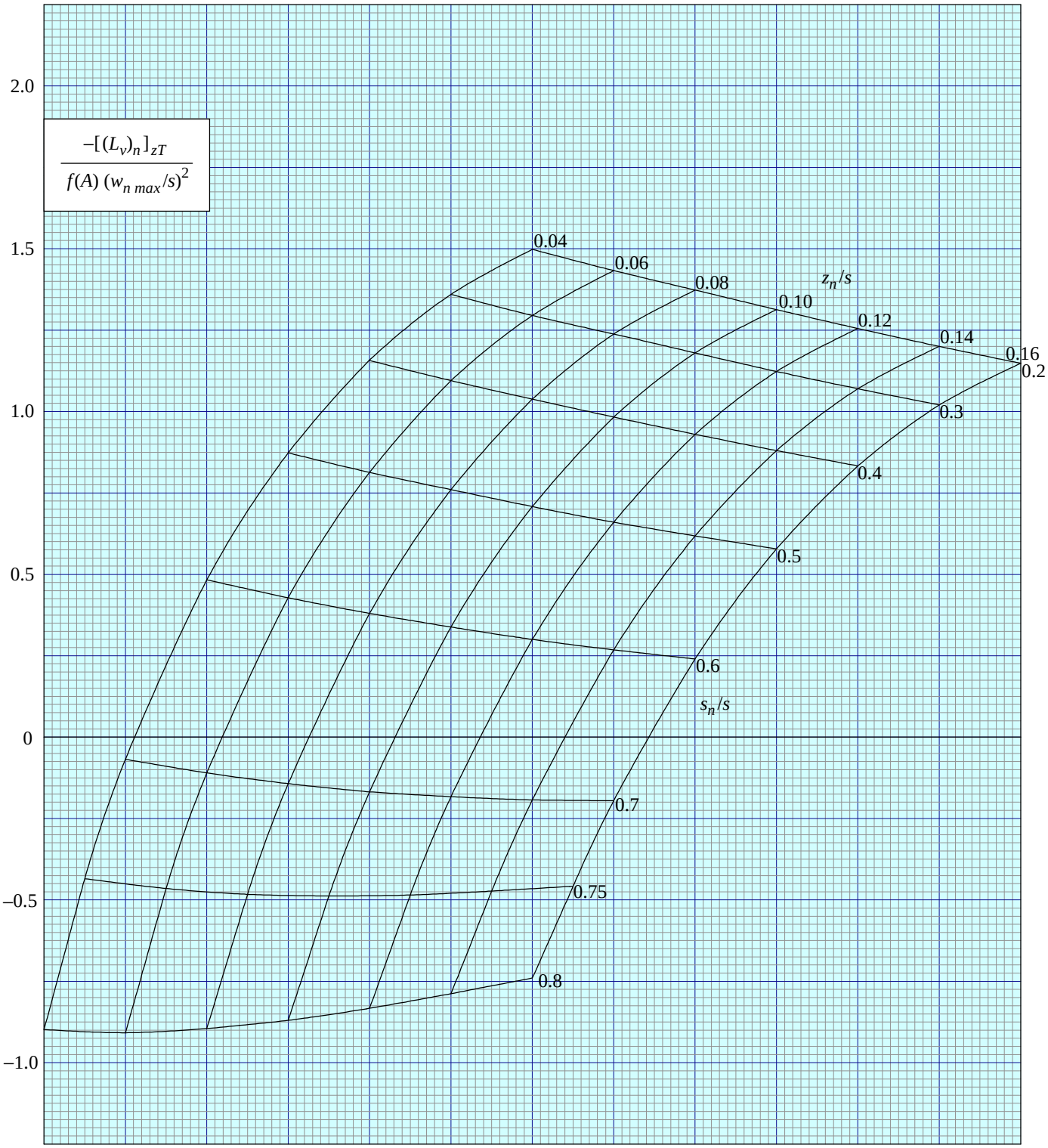

FIGURE A1

This page Amendment C

THE PREPARATION OF THIS DATA ITEM

The work on this particular Item, which supersedes Item No Aero A.06.01.05, was monitored and guided by the Aerodynamics Committee which first met in 1942 and now has the following membership:

Chairman

Mr E.C. Carter	–	Aircraft Research Association

Vice-Chairman

Dr G.M. Lilley	–	Southampton University

Members

Prof. L.F. Crabtree	–	Royal Aircraft Establishment
Mr R.L. Dommett	–	Royal Aircraft Establishment
Mr H.C. Garner	–	Royal Aircraft Establishment
Mr J.R.C. Pedersen	–	British Aircraft Corporation Ltd, Stevenage
Mr J.J. Perrin	–	Aérospatiale, Châtillon
Mr M.R. Pike	–	Rolls-Royce (1971) Ltd, Derby
Mr M.W. Salisbury	–	British Aircraft Corporation Ltd
Mr J. Taylor	–	Hawker Siddeley Aviation Ltd, Woodford
Mr J.W.H. Thomas	–	Hawker Siddeley Aviation Ltd, Hatfield
Mr J. Weir	–	Salford University.

The member of staff of the Engineering Sciences Data Unit concerned is:

Mr P.D. Chappell	–	Head of Aircraft Motion Group.